Rotational spectroscopy in the v3 = v6 = 1 and v6 = 2 vibrational states of CH35Cl3

Adina Ceausu-Velcescu, Petr Pracna, Roman Motiyenko, Laurent Margules

Rotational spectroscopy in the v_3=v_6=1 and v_6=2 vibrational states of $CH^{35}Cl_3$

Adina CEAUSU – VELCESCU*, Petr PRACNA[†], Roman A. MOTIYENKO, Laurent MARGULES[§]

*Université de Perpignan, Laboratoire de Mathématiques et Physique, 52 Avenue Paul Alduy, 66860 Perpignan Cedex, France

[†] University of Chemistry and Technology, Department of Analytical Chemistry, Technická 5, 166 28 Prague 6, Czech Republic

[§] Univ. Lille, CNRS, UMR 8523 - PhLAM - Physique des Lasers Atomes et Molécules, F-59000 Lille, France

Proofs to: Dr. Adina CEAUSU-VELCESCU
Université de Perpignan,
Laboratoire de Mathématiques et Physique,
52 Avenue Paul Alduy, 66860 Perpignan Cedex France
Tel. (0033)4 68 66 22 19
Fax: (0033)4 68 66 22 34
E-mail address: adina@univ-perp.fr

Tables: 5

Figures: 4

Keywords: chloroform, high-resolution MMW spectroscopy, excited vibrational states

Abstract

The overtone v_6=2 (~520 cm^{-1}) and combination v_3=v_6=1 (~627 cm^{-1}) vibrational levels of chloroform $CH^{35}Cl_3$ have been studied by millimeter wave spectroscopy, in the regions 150-330 and 360-660 GHz, corresponding to J=22-49 and 55-99. Like the v_6=1 fundamental vibration, the v_3=v_6=1 combination level has an accidentally small value of C-B-$C\zeta$ ~ –0.0029 cm^{-1}. Hence, a global q_{22} resonance (Δk=Δl=±2) connects the (k-1, l_6= -1) and (k+1, l_6=+1) sublevels. As a consequence, several resonant q_{12} (Δk=±1, Δl=∓2) crossings occur, which enabled the precise determination of the q_{12} interaction parameter for this state. Altogether, 1182 rotational transitions in the v_3=v_6=1 combination level have been measured and fitted, with a standard deviation of 41.2 kHz.

For the v_6=2 (A_1+E) overtone level, the combined effects of the q_{22} and q_{12} l-type interactions induce resonant crossings between the (k, l_6=0)/(k+1, l_6=-2) pairs of levels, for a large variety of k values. Altogether, 1463 rotational transitions in the (l_6=0) A_1 sublevel and 2924 rotational transitions in the (l_6=±2) E sublevels, together with nine perturbation-allowed transitions induced by the q_{12} (Δk=±1, Δl=∓2) interaction, have been measured and fitted, with a global standard deviation of 41.4 kHz. This resulted in the first accurate determination of the molecular constants of this overtone level.

1. Introduction

$CHCl_3$ (chloroform, trichloromethane) is a clear, colorless, highly volatile, non-flammable liquid at room temperature. It is widely used as an extraction solvent for fats, oils, greases, rubber, resins, lacquers, artificial silk manufacture, gums and adhesives. Chloroform is also employed as an industrial solvent in the extraction and purification of some antibiotics, alkaloids, vitamins and flavors [1]. This explains why most of the oldest investigations of its vibrational spectrum were done in the liquid phase.

Chloroform may be hazardous to the environment, as it can be transported in air as vapor and dissolved in water. In the air, chloroform eventually breaks down to other toxic chemicals, such as phosgene and hydrogen chloride.

Gas-phase spectroscopy is an invaluable tool for monitoring atmospheric pollutants [2]. Unfortunately, with several low-lying excited states, small rotational constants, and four isotopologues simultaneously present, the gas-phase high-resolution infrared spectra of natural chloroform are almost impossible to interpret. The use of (expensive) isotopically pure samples seems thus to be the only possibility.

Rotational spectra of the symmetric species, in the ground vibrational state and the low-lying vibrational states v_2=1 (676 cm^{-1}), v_3=1 (367 cm^{-1}), and v_6=1 (260 cm^{-1}), were studied by Carpenter *et al.* [3]. The ground vibrational state was also studied using millimeter and submillimeter-wave spectroscopy by Cazzoli *et al.* [4], who obtained very accurate centrifugal distortion constants. For the main isotopologue $CH^{35}Cl_3$, these authors also resolved the splitting of the K=3 transitions, for $J \geq 45$, and obtained thus a value of the h_3 ($\Delta k = \pm 6$) interaction parameter in the ground state. Colmont *et al.* [5] analyzed the ground state rotational spectra of various isotopic species of chloroform and obtained empirical experimental and *ab initio* structures. Later, Demaison [6] recalculated the *ab initio* equilibrium structure and derived also, as a check, a semi-experimental equilibrium structure.

Rovibrational studies were performed for all fundamental bands of $CH^{35}Cl_3$ [7, 8, 9, 10, 11] including recently the ν_6 fundamental vibration, located near 260 cm^{-1} [12]. The latter study, which merged rovibrational wavenumbers of the ν_6 band and rotational data from a previous work of Margulès *et al.* [13] in a global least-squares fit, comprises also a first accurate determination of the axial ground state constants C_0, D_K^0, and H_K^0. Unfortunately, the infrared study of the $2\nu_6$ lowest overtone levels was not possible so far due to very low intensities of both the overtone and hot bands reaching this level.

The aim of the present study is thus to provide a first accurate parameter set for the v_6=2 overtone levels of $CH^{35}Cl_3$, near 520 cm^{-1}, through the analysis of the rotational spectrum, which has been recorded on a natural sample. In fact, contrarily to the infrared vibration-rotation spectra, where the high congestion imposes the use of rather expensive isotopically pure samples, the rotational (millimeter-wave) spectrum of a natural sample may present several distinct regions where the contributions of the different isotopologues and vibrational levels of a given isotopologue occur.

The present study includes also a detailed analysis of the rotational spectrum of $CH^{35}Cl_3$ in the v_3=v_6=1 combination level, near 627 cm^{-1}. This combination vibration has been already analyzed through a high-resolution study of the IR $\nu_3+\nu_6-\nu_6$ hot band, in the ν_3 region, near 367 cm^{-1} [9]. In this study, Pietilä *et al.* assigned 199 peaks of the above mentioned hot band, the wavenumbers of which were fitted using a fourth-order polynomial in m[1]. However, the two components (l_6=-1 and l_6=+1) of this bi-parallel band were treated separately, the strong l(2,2) interaction, present both in the lower and the upper levels, being absorbed into effective $B(\pm l)$ constants. The authors further remarked that the resonance was almost exact, since the difference $B(-l)$-$B(+l)$=237(3)×10^{-6} cm^{-1} almost equals 4|q_{22}|=243.87(4)×10^{-6} cm^{-1}. Thus, the aim of the present study is to provide a more accurate treatment of this combination level with explicit inclusion of the l-type interactions, resulting in accurate molecular parameters, necessary to further studies of merged IR and rotational data.

2. Experimental details

The measurements in the frequency range under investigation (150-660 GHz) were performed on a chloroform sample with natural abundance, using the Lille spectrometer [14]. The absorption cell was a stainless-steel tube (6 cm diameter, 220 cm long). Measurements were conducted at room temperature and at a sample pressure of about 30 Pa. The frequency ranges 150-330 and 360-660 GHz were covered with various active and passive frequency multipliers from VDI Inc. and an Agilent synthesizer (12.5-18.25 GHz) was used as the source of radiation. In order to improve the signal sensitivity, the sources were frequency modulated at 30.5 kHz and lock-in detection with the second harmonic was used. Typical estimated uncertainties for measured line frequencies are 30 to 50 kHz, depending on the observed S/N ratio and the frequency range.

[1] Where, as usual, m= - J for a P transition (ΔJ=-1) and J+1 for a R transition (ΔJ= +1).

Despite the rather low pressure used in the experiment, we could not achieve Doppler-limited linewidths, for at least two reasons: (i) The hyperfine structure (HFS), which is still apparent for rotational lines with intermediate *J*/high *K* values. Many of the observed lines are thus partially or completely unresolved hyperfine structure components, even at Doppler linewidth. (ii) The increase of the frequency modulation depth during the experiment, which was necessary for improving the S/N ratio, for a better observation of transitions pertaining to the excited vibrational states. This increase resulted in additional broadening, giving for instance linewidths of the order of 1 MHz in the intermediate *J*-values region (compared to an estimated Doppler linewidth of the order of 0.3 MHz). Consequently, broader intermediate-*J*/low-*K* lines, with no apparent HFS, were included in the least-squares fit with higher uncertainties, whereas weaker, intermediate-*J*/high-*K* lines, showing partly resolved HFS, were excluded from the fit (as explained later).

3. The rotational spectrum

The degenerate fundamental vibration v_6=1 (CCl_3 asymmetric bending vibration), located at 260.6 cm^{-1}, is well separated from other vibrational levels and could be therefore treated as isolated [12, 13]. This is also the case of the v_6=2 (A_1+E symmetry) and v_3=v_6=1 (E) levels, which are separated by more than 100 cm^{-1}.

We started assignments with the rotational transitions in the v_3=v_6=1 level. Like the v_6=1 fundamental vibration, the v_3=v_6=1 combination level is characterized by an accidentally small value of $|C - B - C\zeta| \approx 88\,MHz$. This combination of constants determines the separation of **unperturbed** (*K*-1, l_6=-1)/(*K*+1, l_6=+1) levels coupled by the q_{22} *l*-type resonance [13], which is roughly given by $\Delta E \approx 4(C - B - C\zeta)K \approx -0.012K$ (in cm^{-1} units). This separation increases only slowly with *K*, whereas the *l*(2,2) coupling matrix elements rapidly increase with *J*. This confers to the q_{22} interaction a globally resonant character, which is for vibrational levels with $(C - B - C\zeta) \approx B$ 'reserved' to the *kl*=+1 sublevels only. The q_{22} resonance produces an effective contribution to the *B* rotational constant $\Delta B \approx \pm 2|q_{22}|$, with the upper sign corresponding to the higher level in the (*K*+1, l_6=+1) / (*K*-1, l_6= -1) pairs of levels in resonance. Thus, the *K*-clusters become wide separated, with the l_6=+1 lines pushed down to lower frequencies and those of l_6=-1 up to higher frequencies. For a given *J*, the *l*(2,2) resonance term decreases with *k*, whereas the unperturbed energies difference increases only slightly with *k*. Hence, the absolute magnitude of the energy shift decreases with *k*, for a given *J*. The, otherwise degenerate, |*kl*=+1, *J*+1> ←

$|kl$=+1, $J>$ transitions are symmetrically split by about $\pm 4|q_{22}|(J+1)$, with the A_- component at lower frequencies. For $kl \neq +1$, due to the negative sign of $(C-B-C\zeta)$, the l_6=+1 lines are pushed down to lower frequencies, whereas the l_6=-1 lines are pushed up to higher frequencies. The displacement decreases with k, for a given J cluster. The combined effects of $D_{JK} < 0$ and of the q_{22} resonance make thus the lower l_6=+1 cluster degraded towards higher frequencies, for all the values of J. The l_6=-1 clusters are degraded towards lower frequencies for $J \leq 35$; a bandhead is observed for moderate J values (Fig. 1), whereas, for higher J values, these clusters become also degraded towards higher frequencies (Fig. 2).

Assignment of the v_3=v_6=1, l_6= −1 and +1, clusters of rotational lines, which much resemble those of v_6=1, was thus straightforward, despite their weakness as shown in Fig. 1. A total of 1182 lines of the l_6=±1 components have been assigned and fitted.

The pattern of rotational transitions in the v_6=2 overtone level is quite different from that of the fundamental level v_6=1. The $l(2, 2)$ resonance connects the triplets of levels (K+2, l_6=+2)/(K, l_6=0)/(K-2, l_6= -2), the relative positions of which are mainly determined by the g_{66} anharmonicity parameter and the combination of the $C\zeta$ and (C-B) parameters, as follows: $E(K \pm 2, l_6 = \pm 2) - E(K, l_6 = 0) \approx \pm 4(C-B-C\zeta)(K \pm 1) + 4(g_{66} - C\zeta) = \mp 0.012(K \pm 1) + 0.550$ (in cm^{-1} units).

This puts the (K, l_6=0) levels below their (K-2, l_6= -2) resonance partners for all values of K. Also, the (K, l_6=0) levels lie below the (K+2, l_6=+2) ones for $K < 45$.

The appearance of the K-clusters of rotational lines, for a given J value, in the v_6=2 level, can be easily understood again by considering the case of exact resonance, which concerns the $|0^0\rangle$ and $|\pm 2^{\pm 2}\rangle$ levels, the latter being degenerate. The Wang transformation yields an A_+ block of interacting levels, symmetrically displaced with respect to the mean value of their unperturbed energies, and a $|2^2, A_-\rangle$ unperturbed level. Hence, the (2^2, A_-, J+1)← (2^2, A_-, J) transition is unperturbed. Three clusters can thus be observed, for each value of J (Fig. 1): a lower-frequency one, which corresponds to l=0, a middle one, composed of l=+2 transitions, which 'follows' the (2^2, A_-, J+1)← (2^2, A_-, J) transition, and a higher-frequency one, composed of l= -2 transitions and 'following' the (2^2, A_+, J+1)← (2^2, A_+, J) transition. This latter cluster contains also the (1^2) and (0^2) transitions. The effect of the $l(2,2)$ resonance on the appearance and behavior of the l=0, +2, and -2 J-clusters of lines is by the way nicely depicted in Fig. 5 of Ref. [15], for the v_{10}=2 rotational spectrum of CF_3CCH.

The lower frequency clusters, corresponding to l_6=0 and composed of regularly spaced lines, degraded to higher frequencies, were clearly observed in the spectrum, distinct from the much stronger rotational transitions of the vibrational ground state and the fundamental v_6=1 level, not being obscured by them (Figs. 1 and 2). Assignment of the l_6=0 transitions at moderate J-values (Fig. 1), facilitated by the intensity alternation due to nuclear spin statistics, was the starting point of the analysis, yielding more reasonable values of the $B^{(0)}$ and $B^{(2)}$ rotational constants, which were used for further assignments. At this stage, the AABS package, designed by Kisiel *et al.* for broadband rotational spectroscopy [16], has been extensively used. Finally, the middle and the upper clusters, corresponding to l_6=+2 and l_6= -2, respectively, were also assigned. Like before, intensity alternation due to nuclear spin statistics and the Loomis-Wood representation of the spectrum in the AABS package were extremely helpful in progressive extension to higher J values. A total of 1463 lines of the l_6=0 component and 2924 lines of the l_6=±2 components ($22 \le J'' \le 49$ and $55 \le J'' \le 99$) have been thus assigned and fitted.

With the energies of the l_6=0 levels being pushed down by the q_{22} resonance, these fall into local resonances with both l_6=+2 and l_6=-2 levels due to other vibration–rotation interactions, such as q_{12} (Δk=±1, Δl=∓2), but also higher-order f_{42} (Δk=±4, Δl=∓2) and f_{52} (Δk=±5, Δl=±2) interactions. In addition to this, resonant crossings between the l_6=+2 and l_6= -2 levels due to the f_{14} interaction occur for several low K values, as shown in Figure 3 with the reduced energy plot of the whole system of rotational levels of v_6=2. Nine perturbation-allowed transitions, induced by the q_{12} interaction, were also included in the fit.

4. Results and discussion

For fitting the experimental frequencies, a conventional Hamiltonian of a symmetric-top molecule has been used, the matrix elements of which are given in Appendix A. For the least-squares fitting, using the SIMFIT program [17], the data were given statistical weights proportional to the inverse square of their estimated uncertainties.

The present work is based on a huge set of rotational data. Part of the observed transitions would be further split by the hyperfine quadrupole interactions due to the three chlorine nuclei with nuclear spin 3/2. The detailed description of the tensorial coupling techniques allowing to construct the nuclear quadrupole part of the Hamiltonian, for any number of nuclei of spin ≥1, can be found for instance in Refs. [18, 19]. This tensorial coupling mechanism is implemented in the SPFIT/SPCAT program package [20], which was

already used for studying the HFS of the J=1←0 and J=2←1 transitions in the ground vibrational state of $CHCl_3$ [21]. This structure is quite complex, extending over more than 50 MHz and consisting of a great number of measurable components. The analysis performed by the authors of Ref. [21] allowed fitting all determinable components of the inertial nuclear splitting tensors for the chlorine nuclei. On the contrary, there are only few studies dealing with HFS of rotational transitions in degenerate excited states of symmetric top molecules [3, 22]. For the v_6=1 state of $CHCl_3$, Carpenter *et al.* [3] constrained the eQq_{ZZ} and η_Q parameters to the corresponding ground state values.

In our current analysis we could in principle attempt either at assigning the resolved HFS and fit them explicitly with the SPFIT program, or reducing the resolved HFS to ´hyperfine-free´ rotational frequencies, using e.g. the HFS parameters constrained to their ground vibrational state values, and fit them with the use of SIMFIT program [17]. Our moderate J-values ($22 \leq J'' \leq 35$) spectrum clearly shows hyperfine quartets in the vibrational ground, v_3=1, and v_6=1 states, for high K values, as, for a given J, the quadrupole splitting of lines increases with K. At the same time, intensities are decreasing with increasing K; this makes the quartets of the, much weaker, v_6=2 band, more difficult to distinguish, as they are often overlapped by other, stronger, transitions. For such J-values, HFS structure is already partly collapsing, even though still visible. This means, however, that the reliable assignments of the hyperfine components for using them in either of the mentioned fitting approaches, remains somewhat problematic. Therefore we decided to exclude from the data set the lines corresponding to these intermediate J / high K-values, showing partly resolved hyperfine structure, and those only broadened due to hyperfine interaction give lower weights (i.e. higher uncertainties of 100-200 kHz) and fit them with the SIMFIT program.

Despite this reduction of the data set, frequent overlaps with much stronger transitions in the lower lying levels and of course vanishing intensities for growing J values, we were still able to collect over 1000 transitions in the two l-sublevels of the v_3=v_6=1 vibrational state and over 4000 transitions in the three l-sublevels of the v_6=2 vibrational state, which we believe to be a sound basis for determination of parameters of the centrifugal distortion expansion and all relevant off-diagonal interaction terms of the effective rotational Hamiltonian of a symmetric top molecule.

4.1. The v_3=v_6=1 level

In the v_3=v_6=1 vibrational level, situation is almost the same as that described for v_6=1 [13]: the q_{22} resonance pushes the pairs of interacting levels (k, l_6=-1)/(k+2, l_6=+1) apart so that they are brought into local resonances due to the q_{12} l-type interaction. We were able to detect and assign transitions on both sides of the crossings for the pairs of levels $1^{+1}/2^{-1}$ (at J=43/44) and $3^{+1}/4^{-1}$ (at J=67/68) only: the $2^{+1}/3^{-1}$ crossing, occurring at J=56/57, is in a spectral range not recorded by our spectrometer, whereas the crossings $4^{+1}/5^{-1}$, $5^{+1}/6^{-1}$, and so on, occur at J values which are too high for detecting the corresponding transitions.

The fits were performed with two reduced forms of the effective rotational Hamiltonian, the Q and D reductions [23]. With 14 refined parameters (out of 22), these reduction schemes provided an identical reproduction of the data, with a standard deviation of 41.2 kHz (Table 1). We have to notice that the C, D_K, and η_K coefficients of the K-dependent part of the rotational energies were kept fixed, in order to avoid too high correlation between these parameters and $C\zeta$, the latter parameter being refined.

The unitary equivalence checking of the Q and D reductions, up to 3rd order is shown in Table 2. The results of this Table can be compared to those presented for the v_6=1 level, given in Table 3 of Ref. [12]. Surprisingly, the discrepancies noticed for v_6=1, for instance that between $-2q_{12}^D/F$ and $\frac{1}{2}d_t^Q/q_{22}$, seem to be less important for the v_3=v_6=1 level: for the latter level, the above mentioned quantities agree within 2σ. The 3rd order combinations also show quite good agreement, except the $\Delta^{Q,D}\eta_J$ difference, which is statistically not defined.

4.2. The v_6=2 level

For each value of the rotational quantum number J, rotational levels are grouped into three-level-systems with the same value of G=|k–l|. Several kinds of level crossings take place, but only two of them result into resonances due either to $\Delta(k-l)=3$ or to $\Delta(k-l)=6$ interactions, which have strong, local effects on energy levels with a large variety of G values.

First, the q_{22} resonance pushes the pairs of levels (k, l_6=0)/(k-2, l_6=-2) apart, so that local resonances due to the q_{12} interaction (ΔG=±3) occur (Fig. 3). We have observed such crossings between (k, l_6=0)/(k+1, l_6=-2) levels for a large variety of k values and were thus able to refine not only the main interaction parameter, q_{12}, but also the parameter of the l-dependent term, q_{12}^l, which is of the same order of magnitude as q_{12} [24].

Second, the (k, l_6=0)/(k+4, l_6=-2) levels are interacting through a f_{42} l-type interaction (Δk=±4, Δl=∓2). Level crossings occur for J=60 in the $0^0/4^{-2}$ pair, 71 in the $1^0/5^{-2}$ pair, 81 in the $2^0/6^{-2}$ pair and so on. Unfortunately, only the first crossing occurs at a J-value which is low enough for observing transitions with a reasonable intensity.

Another interesting phenomenon, due to the strong l(2,2) resonance and the resulting mixing of states, occurs: for each G value, G≥45, the two lower levels in the three-level-system (i.e. (k, l_6=0) and (k+2, l_6=+2) change their relative positions, though they do not cross in a conventional sense. This phenomenon has been already described for the v_{10}=2 state of 1,1,1-trifluoropropyne by Wötzel *et al.* [25]. Thus, for a certain value of J, the mixing of the $|k, l_6 = 0\rangle/|k+2, l_6 = +2\rangle$ wavefunctions is so strong that an unambiguous labeling of the levels is not possible. For higher values of J, the labeling becomes again unambiguous, but with reversed ordering of the levels.

The approach employed in the present work for fitting the frequencies of the assigned transitions is that proposed by Sarka and Harder [24], who developed, for an isolated v_t=2 level of a C_{3v} symmetric-top molecule, five reduced forms of the effective Hamiltonian. The common feature of these reduced forms is that from the four lower order $\Delta(k\text{-}l)$=3 interactions, two have to be constrained and the other two refined, but the simultaneous constraint of the k- and l-dependent terms of the (2,-1) interaction is not allowed. Therefore, the following constraints have been suggested up to fifth order [24]: all parameters of the K-dependent terms of off-diagonal interactions (f_{22}^K, f_{12}^K, f_{12}^{lK}, f_{22}^{lK}, ε_K, d_t^K) and the parameter f_{14} of the (4,1) interaction should be fixed to zero. In the present case, all these constraints have been applied except for f_{22}^K (see below). Indeed, it has been shown by Watson *et al.* [23] that the constraint $\tilde{f}_{22}^K = 0$ should be avoided if $|C - B - C\zeta|$ is accidentally too small. This is the case for the $2\nu_6$ vibration of $CHCl_3$ (and situation was of course the same for ν_6 [12]), where $C - B - C\zeta \approx -92\,MHz$. For accidentally small values of $(C - B - C\zeta)$, one can alternatively use one of the following constraints: $\tilde{\tau}_J = 0$, or $\tilde{\tau}_{JK} = 0$, or $\tilde{\tau}_K = 0$.

The reduction schemes employed in the present work correspond to the Q, D, and L reductions described in Ref. [24]. As pointed out in this Reference, the parameters $\tilde{f}_{14}$, $\tilde{f}_{12}^{lJ}$, $\tilde{f}_{12}^{lK}$, $\tilde{f}_{22}^{lK}$ depend on the transformation parameters o, p, r and therefore three of them should be constrained. The constraints suggested in the above mentioned Reference are thus $\tilde{f}_{14} = 0$; $\tilde{f}_{12}^{lK} = 0$; $\tilde{f}_{22}^{lK} = 0$, the $\tilde{f}_{12}^{lJ}$ parameter being refined. In the present case, the f_{24} interaction

parameter (Δk=±2, Δl=∓4) was not refined in the final stage of the calculations but kept fixed to a value obtained in a preliminary stage (see footnote b of Table 3).

With the final choice of 28 refined parameters, the data could be reproduced within error limits comparable to the estimated experimental accuracy, of 50 kHz. The global standard deviation is thus of 41.4 kHz for the three reductions *D*, *Q*, and *L* (Table 3).

The unitary equivalence of the three parameter sets, up to third order, was also checked and the results are presented in Table 4. For this purpose, the following relations, derived for the lowest order parameters of the $\Delta(k\text{-}l)$=3 interactions, have been employed [26]

$$-\frac{2q_{12}^{D}}{F}=\frac{d_t^{Q}}{2q_{22}} \qquad \frac{d_t^{L}}{2q_{22}}=\frac{2q_{12}^{l,D}}{G}$$

$$q_{12}^{l,D}=q_{12}^{l,Q}+\frac{Gd_t^{Q}}{4q_{22}} \qquad q_{12}^{L}=q_{12}^{D}+\frac{Fq_{12}^{l,D}}{G}$$

As shown in Table 4, the above equalities are satisfactorily, though not perfectly, fulfilled. Good fulfillment of the unitary equivalence of parameters occurs also for the third-order constants η_J and η_K, for which the following equalities can be established [26]:

$$\Delta^{Q,D}\eta_J=-\Delta^{\mathrm{Q,D}}\eta_K=-\frac{8(q_{12}^{D})^2}{F}=-\frac{\left(d_{\mathrm{t}}^{Q}\right)^2F}{2q_{22}^2}$$

$$\Delta^{Q,L}\eta_J=-\Delta^{Q,L}\eta_K=-\frac{8(q_{12}^{L})^2}{F}=-\frac{8\left(q_{12}^{l,Q}\right)^2F}{G^2}$$

$$\Delta^{L,D}\eta_J=-\Delta^{L,D}\eta_K=\frac{8[(q_{12}^{L})^2-(q_{12}^{D})^2]}{F}$$

In these relations, the symbol $\Delta^{X,Y}$ implies the difference between the values of a parameter in the *X* and *Y* reductions (*X*,*Y* = *Q*, *D*, or *L*). By the way, the refinement of the f_{22}^{lK} parameter has a noticeable effect on the third-order parameters η_J and η_K, thus improving the fulfillment of the above mentioned equalities.

We have not shown the unitary equivalence relations for the fourth-order parameters f_{22}^{J} and f_{42}, as suggested for instance in Ref. [26], because the corresponding differences are only poorly defined. It would be however interesting to check, even only partly, the fourth order contributions to the rotational constants *B* and *C*. The dependence of these rotational constants on the transformation parameter *s* writes ([26], corrected in [27]):

$$B_{v,l}(s)=B_{v,l}+4\left[\frac{1}{2}(v^2-l^2)+v\right]\left(q_{12}s+\frac{1}{4}Fs^2\right)-4(v^2+2v-3l^2)\left(q_{12}^{l}s-\frac{1}{4}Gs^2\right)$$

$$C_{v,l}(s)=C_{v,l}-8\left[\frac{1}{2}(v^2-l^2)+v\right]\left(q_{12}s+\frac{1}{4}Fs^2\right)$$

From these relations, one can derive for a v_t=2 state the following equalities:

$$\Delta^{Q,D}B^{(0)} = -16\left[\frac{(q_{12}^{D})^2}{F} + 2\frac{\left(q_{12}^{l,D}\right)^2 - \left(q_{12}^{l,Q}\right)^2}{G}\right]$$

$$\Delta^{Q,D}B^{(2)} = -8\left[\frac{(q_{12}^{D})^2}{F} - 2\frac{\left(q_{12}^{l,D}\right)^2 - \left(q_{12}^{l,Q}\right)^2}{G}\right]$$

as well as

$$\frac{1}{2}\Delta^{Q,D}C^{(0)} = \Delta^{Q,D}C^{(2)} = 16\frac{(q_{12}^{D})^2}{F}$$

For the *C* constants, checking of the above equalities is meaningless, the uncertainties being larger than the experimental differences. For the Δ*B* values however, good fulfillment is observed, even though uncertainties of the experimental differences are of the same order of magnitude as the differences themselves. We obtain for instance for the l_6=0 sublevel, $\left(\Delta^{Q,D}B^{(0)}\right)_{exp} = 5.27(188)\times10^{-9}$ cm^{-1} and $\left(\Delta^{Q,D}B^{(0)}\right)_{th} = 4.701(62)\times10^{-9}$ cm^{-1}. For the l_6=±2 sublevels, we obtain $\left(\Delta^{Q,D}B^{(2)}\right)_{exp} = -1.97(116)\times10^{-9}$ cm^{-1} and $\left(\Delta^{Q,D}B^{(2)}\right)_{th} = -1.740(31)\times10^{-9}$ cm^{-1}.

As said previously, the experimental frequencies could be reproduced with a global standard deviation of 41.4 kHz. It should be mentioned, however, that we have not succeeded in reproducing in such a quantitative manner the (*k*=±1, l_6=∓2) and (*k*=±5, l_6=±2) series, as well as the low-*J* (*k*=±3, l_6=0) transitions, which were excluded from the final fits.

These series connect levels pertaining to the nine-level system (0^0, A_+), (3^0, A_+/A_-), (1^{-2}, A_+/A_-), (2^2, A_+/A_-) and (5^2, A_+/A_-) in which the higher-order diagonal splitting terms f_{24} and h_3 compete with the, much stronger, q_{22} and q_{12} resonances. These latter resonances act globally all over the system of rotational levels of v_6=2, the q_{12} term producing a series of resonant level crossings. This is illustrated in Fig. 3 and also in a broader *J*/*K* span in the reduced energy diagram included in the Supplementary material.

The interplay of all these interactions produces strongly irregular patterns of the A_+/A_- splittings of the above mentioned series. The independent determination of the parameters of the three $\Delta(k-l)=6$ interactions (i.e. f_{42}, f_{24}, and h_3) would be probably enabled by the observation and inclusion in the fit of transitions with different selection rules, e.g. direct *l*-type resonance transitions, like achieved in analogous studies of the vibrational state v_{10}=2 of CF_3CCH [25] or the vibrational state v_6=2 of $SiHF_3$ [26]. This was unfortunately not the case in the present work as such measurements would have required a completely different

experimental setup, which we did not have at our disposal. As a consequence, the f_{42} and h_3 parameters could be determined, but may still remain correlated. The f_{24} parameter could not be determined and was kept fixed in the final stage of the calculations (as described earlier on page 10).

Nevertheless, the exclusion of the above mentioned low-K series from the final fits did not deteriorate the consistency of the diagonal and off-diagonal parameters of the v_6=2 level with those of v_6=1. This is shown in Table 5, for the reduction Q, by comparing the q_{22}, f_{22}^J, d_t, and f_{42} off-diagonal parameters of the two levels. Inspection of this Table shows an excellent agreement for q_{22}, f_{22}^J, and d_t (within less than 2%), whereas the f_{42} values differ by about 5%. The same difference is obtained for the f_{42} values in the reduction D. Situation is somewhat worse for the off-diagonal parameters of v_3=v_6=1, some of which present larger differences with the corresponding v_6=1 values (Table 5). In this case, excellent agreement is observed for q_{22} and f_{42} (within less than 2%), whereas the f_{22}^J values differ by about 5%, and the d_t values by about 14%.

Supplementary data associated with this article can be found in the online version, at doi: …

5. Conclusions

The present work reports on the first high-resolution study of the v_6=2 (A_1+E) and v_3=v_6=1 (E) vibrational states of the $CH^{35}Cl_3$ molecule through the analysis of the corresponding rotational spectra. The reproduction of the rotational data pertaining to v_3=v_6=1 level is fully quantitative. This is also the case for the majority of the data pertaining to the v_6=2 overtone level, except the (±3,0), (±1,∓2) and (±5,±2) series, where unusually large splittings occur.

Acknowledgements

One of the authors (A. C-V) wishes to thank Drs. Z. Kisiel (Warsaw) and J. Demaison (Lille) for fruitful discussions.

Appendix A. Definition of the matrix elements of the effective vibration-rotational Hamiltonian

The diagonal matrix elements were defined conventionally as

$$\begin{aligned} E_{vr}(J,k,l_t) = {} & E_v + B_v J(J+1) + \left(C_v - B_v\right)k^2 - D_J^v J^2(J+1)^2 - D_{JK}^v J(J+1)k^2 - D_K^v k^4 \\ & + H_J^v J^3(J+1)^3 + H_{JK}^v J^2(J+1)^2 k^2 + H_{KJ}^v J(J+1)k^4 + H_K^v k^6 \\ & + L_J^v J^4(J+1)^4 + L_{JJK}^v J^3(J+1)^3 k^2 + L_{JK}^v J^2(J+1)^2 k^4 + L_{JKK}^v J(J+1)k^6 + L_K^v k^8 \\ & + \left[-2\left(C\zeta_t\right)_v + \eta_{tJ} J(J+1) + \eta_{tK} k^2 + \tau_{tJ} J^2(J+1)^2 \right. \\ & + \tau_{tJK} J(J+1)k^2 + \tau_{tK} k^4 + \sigma_{tJ} J^3(J+1)^3 \\ & \left. + \sigma_{tJK} J^2(J+1)^2 k^2 + \sigma_{tKJ} J(J+1)k^4 + \sigma_{tK} k^6 \right] k l_t \end{aligned} \tag{A1}$$

The following off-diagonal matrix elements were considered

a) *l*-type operators

$$\begin{aligned} & \left\langle v_t^{l_t \pm 2}; J, k \pm 2 \middle| \mathbf{H}_{22} + \mathbf{H}_{24} + \mathbf{H}_{26} \middle| v_t^{l_t}; J, k \right\rangle \\ & = \left[\left(v_t \mp l_t\right)\left(v_t \pm l_t + 2\right)\right]^{1/2} \left\{ q_{22} + f_{22}^J J(J+1) + f_{22}^K \left[k^2 + \left(k \pm 2\right)^2 \right] \right. \\ & \left. + f_{22}^{JJ} J^2(J+1)^2 + f_{22}^{JK} J(J+1)\left[k^2 + \left(k \pm 2\right)^2 \right] + f_{22}^{KK} \left[k^4 + \left(k \pm 2\right)^4 \right] \right\} F_2^{\pm}(J,k) \end{aligned} \tag{A2}$$

$$\begin{aligned} & \left\langle v_t^{l_t \pm 2}; J, k \mp 1 \middle| \mathbf{H}_{22} + \mathbf{H}_{24} \middle| v_t^{l_t}; J, k \right\rangle \\ & = \left[\left(v_t \mp l_t\right)\left(v_t \pm l_t + 2\right)\right]^{1/2} \left\{ \left[q_{12} + f_{12}^J J(J+1) \right]\left(2k \mp 1\right) + f_{12}^K \left[k^3 + \left(k \mp 1\right)^3 \right] \right\} F_1^{\mp}(J,k) \end{aligned} \tag{A3}$$

$$\begin{aligned} & \left\langle v_t^{l_t \pm 2}; J, k \mp 1 \middle| \mathbf{H}_{41} + \mathbf{H}_{43} \middle| v_t^{l_t}; J, k \right\rangle \\ & = \left[\left(v_t \mp l_t\right)\left(v_t \pm l_t + 2\right)\right]^{1/2} \left\{ q_{12}^l + f_{12}^{lJ} J(J+1) + f_{12}^{lK} \left[k^2 + \left(k \mp 1\right)^2 \right] \right\} \left(2l_t \pm 2\right) F_1^{\mp}(J,k) \end{aligned} \tag{A4}$$

$$\begin{aligned} & \left\langle v_t^{l_t \pm 2}; J, k \mp 4 \middle| \mathbf{H}_{24} + \mathbf{H}_{26} \middle| v_t^{l_t}; J, k \right\rangle = \left[\left(v_t \mp l_t\right)\left(v_t \pm l_t + 2\right)\right]^{1/2} \left\{ f_{42} + f_{42}^J J(J+1) \right. \\ & \left. + f_{42}^K \left[k^2 + \left(k \mp 4\right)^2 \right] \right\} F_4^{\mp}(J,k) \end{aligned} \tag{A5}$$

$$\left\langle v_t^{l_t \pm 4}; J, k \mp 2 \middle| \mathbf{H}_{42} \middle| v_t^{l_t}; J, k \right\rangle = \frac{f_{24}}{4} \left[\left(v_t \mp l_t - 2\right)\left(v_t \mp l_t\right)\left(v_t \pm l_t + 2\right)\left(v_t \pm l_t + 4\right)\right]^{1/2} F_2^{\mp}(J,k) \tag{A6}$$

$$\left\langle v_t^{l_t\pm4};J,k\pm1\middle|\mathbf{H}_{42}\middle|v_t^{l_t};J,k\right\rangle=\frac{f_{14}}{4}(2k\pm1)\Big[(v_t\mp l_t-2)(v_t\mp l_t)\times(v_t\pm l_t+2)(v_t\pm l_t+4)\Big]^{1/2}F_1^{\pm}(J,k) \tag{A7}$$

b) $\Delta k=\pm3$ operators

$$\left\langle v_t^{l_t};J,k\pm3\middle|\mathbf{H}_{23}+\mathbf{H}_{25}\middle|v_t^{l_t};J,k\right\rangle=\left\{d_t+d_t^J J(J+1)+d_t^K\left[k^2+(k\pm3)^2\right]\right\}l_t F_3^{\pm}(J,k) \tag{A8}$$

$$\left\langle v_t^{l_t};J,k\pm3\middle|\mathbf{H}_{04}+\mathbf{H}_{06}\middle|v_t^{l_t};J,k\right\rangle=\left\{\left[\varepsilon+\varepsilon_J J(J+1)\right](2k\pm3)+\varepsilon_K\left[k^2+(k\pm3)^2\right]\right\}F_3^{\pm}(J,k) \tag{A9}$$

c) $\Delta k=\pm6$ operator

$$\left\langle v_t^{l_t};J,k\pm6\middle|\mathbf{H}_{06}+\mathbf{H}_{08}\middle|v_t^{l_t};J,k\right\rangle=\left\{h_3+h_3^J J(J+1)+h_3^K\left[k^2+(k\pm6)^2\right]\right\}F_6^{\pm}(J,k) \tag{A10}$$

The notation of the matrix elements of the rotational shifting operators was taken as

$$F_n^{\pm}(J,k)=\prod_{i=1}^{n}\Big[J(J+1)-(k\pm i\mp1)(k\pm i)\Big]^{1/2} \tag{A11}$$

Figure captions

Figure 1. The rotational spectrum of chloroform in the region of J=26←25 transitions. Upper panel: experimental spectrum (natural sample). Lower panel: simulated spectrum, showing several J-clusters of the $CH^{35}Cl_3$ isotopologue, as follows: ground vibrational state – yellow; v_3=1 – gray; v_6=1 – blue; v_3=v_6=1 – black; v_6=2 – red.

Figure 2. The rotational spectrum of chloroform in the region of J=61←62 transitions. Upper panel: experimental spectrum (natural sample). Lower panel: simulated spectrum, showing several J-clusters of the $CH^{35}Cl_3$ isotopologue, with the same color code as for Figure 1. The lines marked with an asterisk are ground state rotational transitions of the $CH^{35}Cl_2{}^{37}Cl$ isotopologue.

Figure 3. Reduced energies (pure J-dependent terms not included) against J, for the v_6=2 levels. Positions of resonant crossings due to q_{12}, f_{42}, and f_{14} interactions are indicated. Dashed arrows indicate interaction between only one of either the A_+ or A_- sublevels.

Figure 4. Hyperfine splittings of the rotational transitions in the v_6=1 level. The J=34, l_6=-1 cluster is shown; the simulated spectrum (lower panel) does not account for these splittings. Several, much weaker, v_6=2 transitions, are indicated by an asterisk.

Table captions

Table 1. Molecular parameters of the v_3=v_6=1 level of $CH^{35}Cl_3$.

Table 2. Demonstration of unitary equivalence between the D and Q reductions, for the v_3=v_6=1 level.

Table 3. Molecular parameters of the v_6=2 level of $CH^{35}Cl_3$.

Table 4. Demonstration of unitary equivalence of the different parameter sets for the v_6=2 level (2^{nd} and 3^{rd} order).

Table 5. Parameters of the (2,2), (3,0) and (4,-2) interactions (in MHz units) in the vibrational states v_6=1, v_3=v_6=1, and v_6=2 of $CH^{35}Cl_3$ (reduction Q).

References

1 http://www.npi.gov.au/resource/chloroform-trichloromethane

2 K. C. Cossel, E. M. Waxman, I. A. Finneran, G. A. Blake, J. Ye, N. R. Newbury, Gas-phase broadband spectroscopy using active sources: progress, status, and applications, Journal of the Optical Society of America B 34(1); 2017: 104-129.

3 J. H. Carpenter, P. J. Seo, D. H. Whiffen, The rotational spectrum of chloroform in its ground and excited vibrational states, Journal of Molecular Spectroscopy 170 ; 1995 : 215-227.

4 G. Cazzoli, G. Cotti, L. Dore, Millimeter and submillimeter-wave spectrum of $CHCl_3$. Determination of the h_3 splitting constant, Chemical Physics Letters 203 ; 1993: 227-231.

5 J.-M. Colmont, D. Priem, P. Dréan, J. Demaison, J. E. Boggs, Rotational spectra of the isotopic species of chloroform: experimental and *ab initio* structures, Journal of Molecular Spectroscopy 191; 1998: 158-175.

6 J. Demaison, Equilibrium structure of chloroform, Journal of Molecular Spectroscopy 251; 2008: 217-219.

7 J. Pietilä, S. Alanko, V.-M. Horneman, R. Anttila, High-Resolution Infrared Studies of ν_1, $2\nu_1$, and $2\nu_4$ Bands of $CH^{35}Cl_3$, Journal of Molecular Spectroscopy 216; 2002: 271-283.

8 R. Paso, V.-M. Horneman, J. Pietilä, R. Anttila, High-resolution study of the infrared band ν_2 of $CH^{35}Cl_3$, Chemical Physics Letters 247; 1995: 277-282.

9 J. Pietilä, V.-M. Horneman, R. Anttila, High-resolution infrared study of the parallel band ν_3 of chloroform $CH^{35}Cl_3$, Molecular Physics 96; 1999: 1449-1456.

10 R. Anttila, S. Alanko, V.-M. Horneman, The C-H bending vibration ν_4 of chloroform $CH^{35}Cl_3$, Molecular Physics 102; 2004: 1537-1542.

11 J. Pietilä, V.-M. Horneman, R. Anttila, B. Lemoine, F. Reynaud, J.-M. Colmont, The perpendicular fundamental ν_5 of chloroform $^{12}CH^{35}Cl_3$: high resolution infrared study of the ν_5 band together with the millimetre-wave rotational spectrum, Molecular Physics 98; 2000: 549-557.

12 P. Pracna, A. Ceausu-Velcescu, V.-M. Horneman, The ground and ν_6=1 vibrational levels of $HC^{35}Cl_3$: The first high-resolution analysis of the ν_6 fundamental band, Journal of Quantitative Spectroscopy and Radiative Transfer 113; 2012: 1220-1225.

13 L. Margulès, J. Demaison, P. Pracna, Rotational spectrum in the ν_6=1 and ν_3=1 levels of chloroform, Journal of Molecular Structure 795; 2006: 157-162.

14 O. Zakharenko, R. A. Motiyenko, L. Margulès, T. R. Huet, Terahertz Spectroscopy of Deuterated Formaldehyde Using a Frequency Multiplication Chain, Journal of Molecular Spectroscopy 317; 2015: 41-46.

15 J. H. Carpenter, M. Motamedi, J. G. Smith, The Millimeter-Wave Rotational Spectrum of CF_3CCH in the Excited Vibrational State v_{10}=2, Journal of Molecular Spectroscopy 171; 1995: 468-480.

16 Z. Kisiel in: J. Demaison *et al.* (Eds.), "Spectroscopy from Space", Kluwer Academic Publishers, Dordrecht, 2001, pp. 91-106; http://info.ifpan.edu.pl./~kisiel/prospe.htm.

17 P. Pracna, K. Sarka, J. Demaison, J. Cosléou, F. Herlemont, M. Khelkhal, H. Fichoux, D. Papousek, M. Paplewski, H. Bürger, High-resolution study of the v_5=1 level of CDF_3, Journal of Molecular Spectroscopy 184; 1997: 93-105.

18 A. A. Wolf, Quitman Williams, and T. L. Weatherly, Hyperfine structure in the microwave spectra of $CFCl_3$ and $CHCl_3$, J. Chem. Phys. 47; 1967: 5101-5109.

19 James E. Wollrab, "Rotational Spectra and Molecular Structure: Physical Chemistry", Academic Press, 1967.

20 H. M. Pickett, The fitting and prediction of vibration-rotation spectra with spin interactions, Journal of Molecular Spectroscopy 148; 1991: 371-377.

21 E. Białkowska-Jaworska, Z. Kisiel, L. Pszczółkowski, Nuclear quadrupole coupling in chloroform and calibration of ab initio calculations, Journal of Molecular Spectroscopy 238; 2006: 72-78.

22 H. S. P. Müller, L. R. Brown, B. J. Drouin, J. C. Pearson, I. Kleiner, R. L. Sams; K. Sung, M. H. Ordu, F. Lewen, Rotational spectroscopy as a tool to investigate interactions between vibrational polyads in symmetric top molecules: low-lying states $v_8 \leq 2$ of methyl cyanide, CH_3CN, Journal of Molecular Spectroscopy 312; 2015: 22-37.

23 J. K. G. Watson, C. Gerke, H. Harder, K. Sarka, Indeterminacies in the $v_t(E)$=1 Levels of C_{3v} Symmetric-Top Molecules, Journal of Molecular Spectroscopy 187; 1998: 131-141.

24 K. Sarka, H. Harder, The reduced effective vibration-rotational Hamiltonian for the v_t=2 levels of C_{3v} symmetric-top molecules, Journal of Molecular Spectroscopy 197; 1999: 254-261.

25 U. Wötzel, H. Mäder, H. Harder, P. Pracna, K. Sarka, The direct *l*-type resonance spectrum of CF_3CCH in the vibrational state v_{10}=2, Chemical Physics 312; 2005: 159-167.

26 M. Gnida, H. Mäder, H. Harder, A. Huckauf, L. Margulès, J. Cosléou, J. Demaison, P. Pracna, K. Sarka, The rotational spectrum of $SiHF_3$ in the vibrational state v_6=2: Observation of direct *l*-type resonance transitions, Journal of Molecular Spectroscopy 216; 2002: 481-492.

27 A. Ceausu-Velcescu, P. Pracna, J. Breidung, W. Thiel, M. Badaoui, The v_4=1 and v_4=2 rovibrational levels of PF_3 revisited: New solutions for old topics, Journal of Molecular Spectroscopy 316; 2015: 11-21.

$v_3 = v_6 = 1$

$v_3 = v_6 = 1$

171600

171700

171800

171900

Frequency / MHz

← *J´* *K´* *l´* <--- *J´´* *K´´* *l´´*

Line 1/ 1: 171719.6809 3.20E-01 26, 8, -1<-- 25, 8, -1 .R 0, 0

merge_bin 0.000 0, 0, 0<-- 0, 0, 0

GS

$v_6 = 1^{+1}$

$v_6 = 1^{-1}$

$v_3 = 1$

$v_6 = 2^{0}$

$v_6 = 2^{-2}$

$v_6 = 2^{+2}$

10^{+1} 19^{+1} 22^{+1} 25^{+1} 23^{-1} 20^{-1} 5^{-1} 0^{-1}

21^{0} 24^{0} 0^{0} 6^{0} 9^{0} 15^{0} 23^{-1} 20^{-1} 17^{-1} 14^{-1} 11^{-1} 8^{-1} 5^{-1} 0^{-1} 2^{2}(A_) 3^{+2} 5^{+2} 8^{+2} 17^{-2} 13^{-2} 7^{-2} 5^{-2} 20^{+2} 2^{-2} 1^{-2}

22^{+1} 25^{+1} 24^{0}

171600 171700 171800 171900

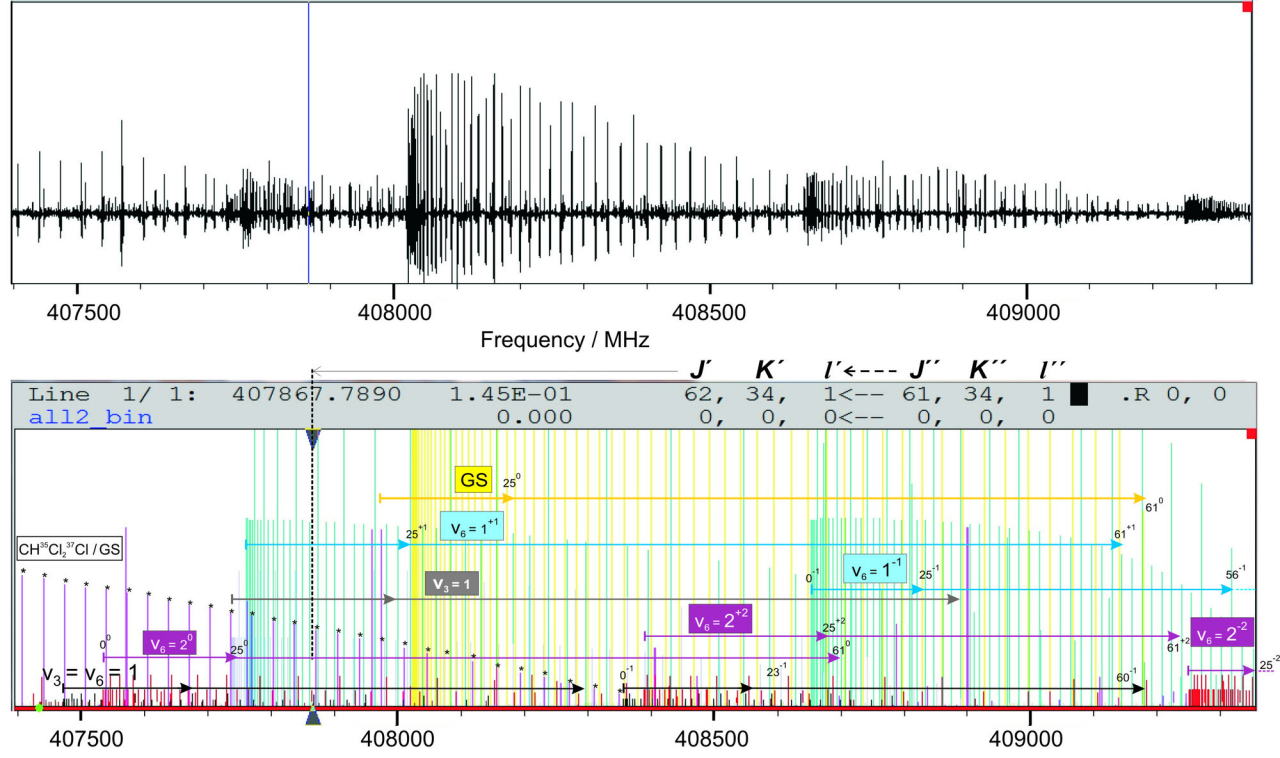
407500
408000
408500
409000
Frequency / MHz
J´ K´ l´←--- J´´ K´´ l´´
Line 1/ 1: 407867.7890 1.45E-01 62, 34, 1<-- 61, 34, 1 .R 0, 0
all2_bin 0.000 0, 0, 0<-- 0, 0, 0
GS
$v_6 = 1^{+1}$
$v_3 = 1$
$v_6 = 1^{-1}$
$v_6 = 2^{+2}$
$v_6 = 2^{0}$
$v_6 = 2^{-2}$
$v_3 = v_6 = 1$
$CH^{35}Cl_2{}^{37}Cl$ / GS
407500
408000
408500
409000

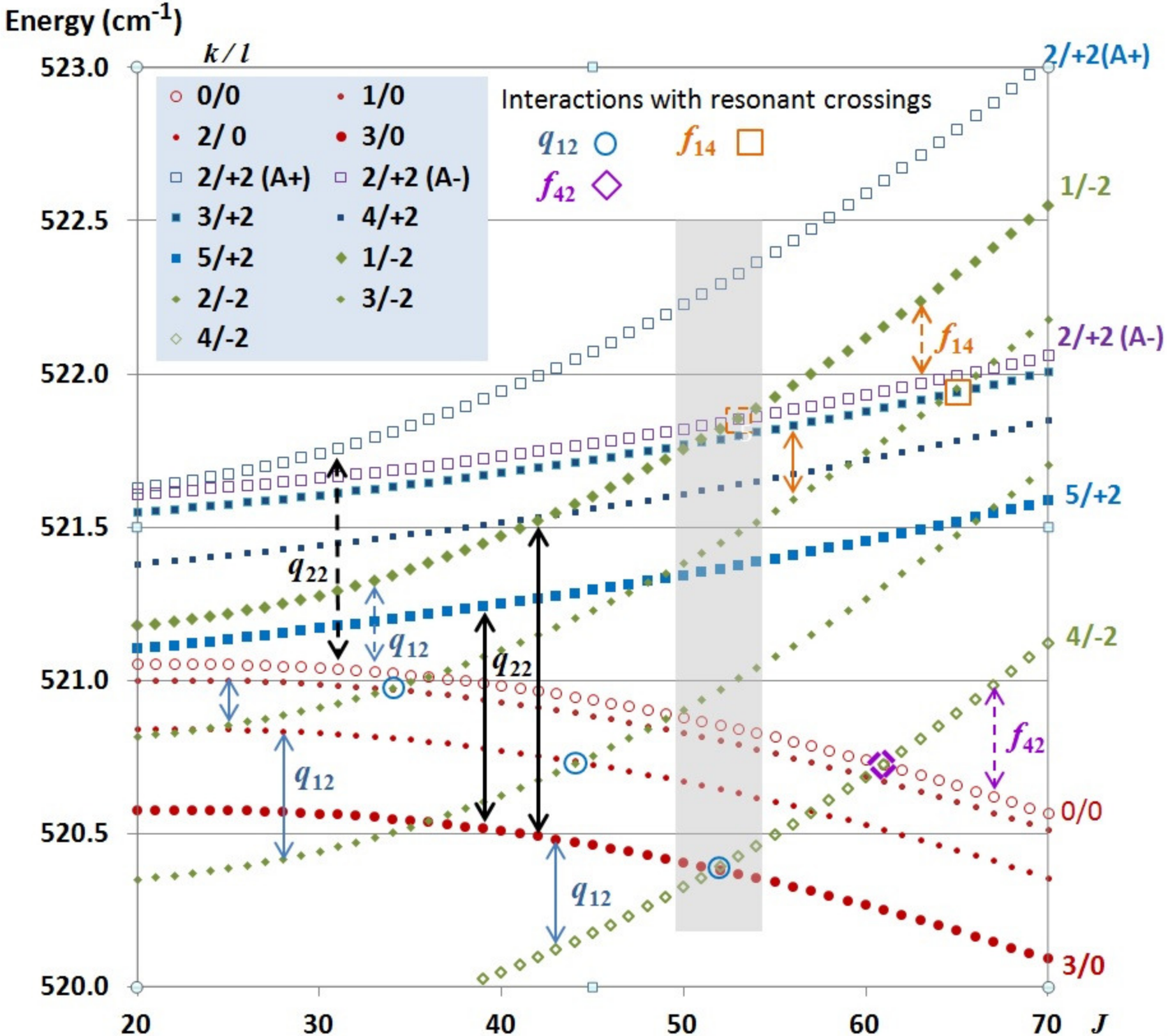
Energy (cm-1)
k / l
0/0
1/0
2/ 0
3/0
2/+2 (A+)
2/+2 (A-)
3/+2
4/+2
5/+2
1/-2
2/-2
3/-2
4/-2
Interactions with resonant crossings
q12
f14
f42
523.0
522.5
522.0
521.5
521.0
520.5
520.0
20
30
40
50
60
70
J
2/+2(A+)
1/-2
2/+2 (A-)
5/+2
4/-2
0/0
3/0
q22
q12
q22
q12
q12
f14
f42

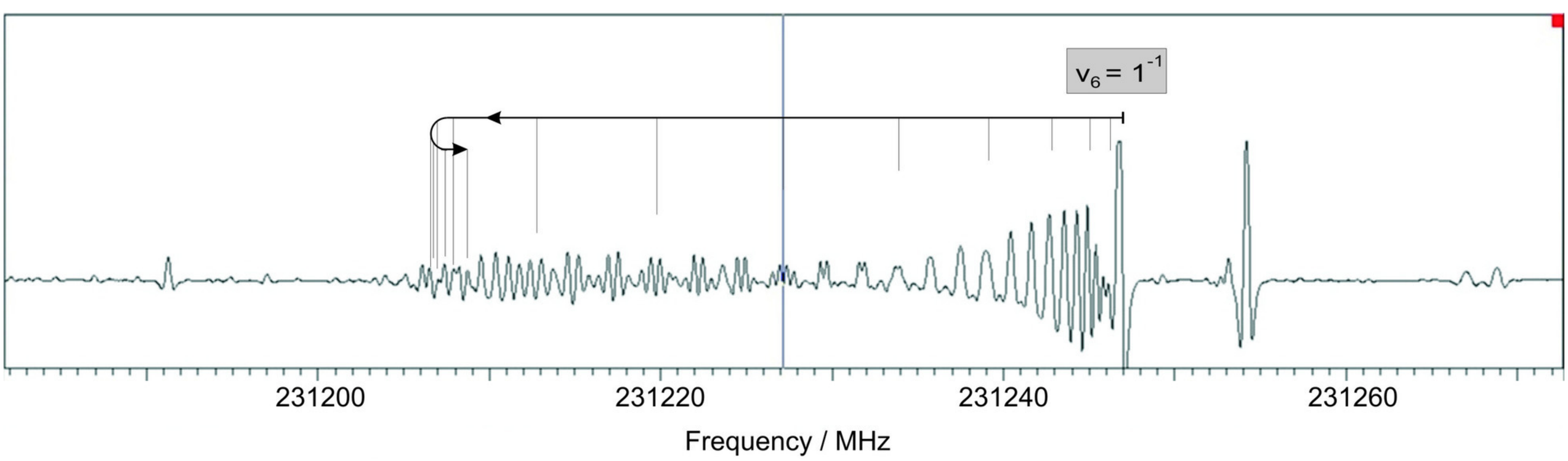
$v_6 = 1^{-1}$
231200
231220
231240
231260
Frequency / MHz

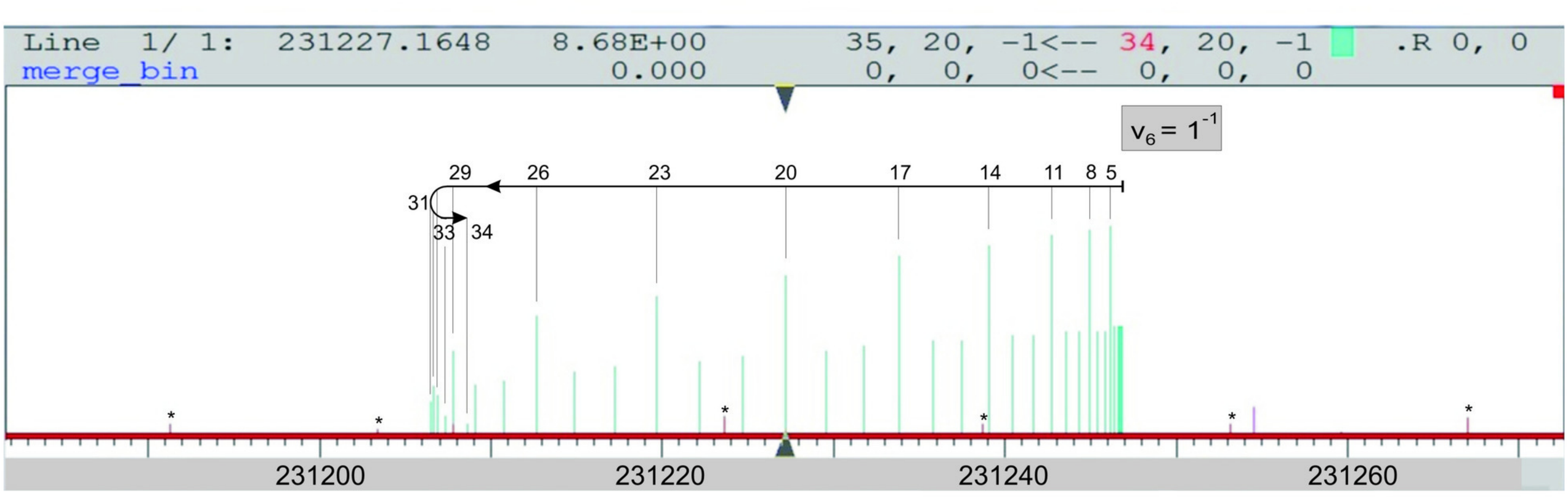
Line 1/ 1: 231227.1648 8.68E+00 35, 20, -1<-- 34, 20, -1 .R 0, 0
merge_bin 0.000 0, 0, 0<-- 0, 0, 0
$v_6 = 1^{-1}$
29 26 23 20 17 14 11 8 5
31
33 34
231200
231220
231240
231260

Table 1. Molecular parameters of the v_3=v_6=1 level of $CH^{35}Cl_3$

Parameter	Reduction *D*	Reduction *Q*
B (MHz)	3301.228 336 (55)	3301.228 335 (55)
C (MHz)	1711.524 214[a]	1711.524 214[a]
D_J (kHz)	1.514 619 (13)	1.514 618 (13)
D_{JK} (kHz)	-2.527 72 (22)	-2.527 71 (21)
D_K (kHz)	0.834 58[b]	0.834 58[b]
H_J (mHz)	1.256 7 (11)	1.256 6 (11)
H_{JK} (mHz)	-5.092 (22)	-5.089 (22)
H_{KJ} (mHz)	6.96 (22)	6.94 (22)
H_K (mHz)	-2.435[b]	-2.435[b]
L_J (nHz)	-2.538[b]	-2.538[b]
$C\zeta$ (MHz)	-1502.060 8 (84)	-1502.062 4 (84)
η_J (kHz)	-4.407 (20)	-4.392 (20)
η_K (kHz)	3.267 5[b]	3.264 9[b]
q_{22} (MHz)	-1.813 161 (18)	-1.813 154 (18)
f_{22}^J (Hz)	4.051 4 (21)	4.052 9 (21)
f_{22}^K (Hz)	-2.981 (19)	-2.975 (19)
f_{22}^{JJ} (μHz)	-8.677[b]	-8.677[b]
f_{22}^{JK} (μHz)	23.058[b]	23.058[b]
q_{12} (kHz)	-82.07 (17)	0.
d_t (kHz)	0.	0.129 03 (27)
f_{42} (Hz)	0.490 0 (59)	0.493 5 (59)
h_3 (mHz)	0.155 5 (10)	0.155 6 (10)
σ (kHz)	41.2	41.2

[a] Constrained to a value obtained from the GS, v_3=1, and v_6=1 values (Refs. [9] and [12]).
[b] Constrained to the corresponding v_6=1 value quoted in [12].
Numbers in parentheses are standard deviations in units of the last digit quoted.

Table 2. Demonstration of the unitary equivalence between the *D* and *Q* reductions, for the v_3=v_6=1 level

Equation [a]	Unit	Verification
$-2\, q_{12}^{D} / F$	10^{-5}	-3.573 2 (75)
$\frac{1}{2}\, d_t^{Q} / q_{22}$	10^{-5}	-3.558 0 (75)
$-8(\, q_{12}^{D})^2 / F$	10^{-10} cm^{-1}	3.913 (16)
$-\frac{1}{2} F(\, d_t^{Q})^2 / q_{22}^2$	10^{-10} cm^{-1}	3.880 (16)
$(\eta_J^{Q} - \eta_J^{D})$	10^{-10} cm^{-1}	5.1 (94)
$-(\eta_K^{Q} - \eta_K^{D})$	10^{-10} cm^{-1}	0.89[b]

[a] $F = C - B + 2C\zeta$.
[b] Constrained to the value obtained in Ref. [12] for the v_6=1 level.

Table 3. Molecular parameters of the v_6=2 states of $CH^{35}Cl_3$

	Parameter		Reduction D	Reduction Q	Reduction L
l_6=0	B	MHz	3305.138 203 (80)	3305.138 361 (80)	3305.138 006 (80)
	C	MHz	1710.636 4 (37)	1710.636 3 (37)	1710.636 4 (37)
	D_J	kHz	1.520 418 (16)	1.520 426 (16)	1.520 405 (16)
	D_{JK}	kHz	-2.545 53 (14)	-2.545 54 (14)	-2.545 54 (14)
	D_K	kHz	0.834 58[a]	0.834 58[a]	0.834 58[a]
	H_J	mHz	1.284 09 (96)	1.284 16 (96)	1.284 00 (96)
	H_{JK}	mHz	-5.172 8 (71)	-5.172 9 (71)	-5.173 5 (71)
	H_{KJ}	mHz	6.902 (20)	6.903 (20)	6.901 (20)
	H_K	mHz	- 2.434 67[a]	- 2.434 67[a]	- 2.434 67[a]
	L_J	nHz	- 2.538[a]	- 2.538[a]	- 2.538[a]
l_6=±2	$4g_{ll}$	MHz	10468.65 (17)	10468.64 (17)	10468.67 (17)
	C	MHz	1710.665 5 (33)	1710.665 5 (33)	1710.665 5 (33)
	D_J	kHz	1.520 277 (10)	1.520 273 (10)	1.520 283 (10)
	D_{JK}	kHz	-2.545 540 (79)	-2.545 535 (79)	-2.545 541 (79)
	D_K	kHz	0.835 04 (20)	0.835 03 (20)	0.835 06 (20)
	H_J	mHz	1.293 13 (60)	1.293 09 (60)	1.293 17 (60)
	H_{JK}	mHz	-5.163 6 (41)	-5.163 4 (41)	-5.163 5 (41)
	H_{KJ}	mHz	6.774 0 (87)	6.773 4 (87)	6.775 2 (87)
	H_K	mHz	- 2.434 67[a]	- 2.434 67[a]	- 2.434 67[a]
	L_J	nHz	- 2.538[a]	- 2.538[a]	- 2.538[a]
	$C\zeta$	MHz	-1502.373 4 (31)	-1502.373 0 (31)	-1502.374 2 (31)
	η_J	kHz	-4.951 4 (18)	-4.942 4 (18)	-5.001 7 (18)
	η_K	kHz	3.238 3 (23)	3.229 3 (23)	3.288 3 (23)
Off-diagonal parameters	q_{12}	kHz	-72.507 (70)	0.	-184.78 (49)
	q_{12}^{l}	kHz	91.50 (40)	150.58 (40)	0.
	$q_{12}^{l,J}$	Hz	-6.541 (88)	-6.602 (88)	-6.445 (87)
	q_{22}	MHz	-1.829 779 5 (77)	-1.829 780 3 (76)	-1.829 778 7 (77)
	f_{22}^{J}	Hz	3.861 4 (14)	3.863 3 (14)	3.865 5 (14)

f_{22}^{K}	Hz	-3.028 6 (19)	-3.029 4 (19)	-3.031 9 (19)
f_{22}^{JJ}	μHz	-8.738 (82)	-8.743 (82)	-8.716 (82)
f_{22}^{JK}	μHz	23.011[a]	23.011[a]	23.011[a]
d_t	kHz	0.	0.114 89 (11)	-0.177 90 (77)
f_{42}	Hz	0.506 69 (45)	0.509 51 (44)	0.510 15 (45)
f_{24}	kHz	-0.661[b]	-0.661[b]	-0.661[b]
h_3	mHz	0.154 14 (99)	0.153 88 (99)	0.154 50 (99)
σ	kHz	41.4	41.4	41.4

[a] Constrained to the v_6=1 values obtained in Ref. [12].
[b] Constrained to a value obtained in a preliminary fit, which still included the (k=1, l_6=-2) lines. These lines were excluded from the final fit (see text).
Numbers in parentheses are standard deviations in units of the last digit quoted.

Table 4

Demonstration of unitary equivalence of the different parameter sets for the v_6=2 level (2nd and 3rd order)

Equation [a]	Unit	Verification	Equation [a]	Unit	Verification
$-2\,q_{12}^{D}\,/\,F$	10^{-5}	-3.153 0 (30)	$2\,q_{12}^{l,D}\,/\,G$	10^{-5}	4.903 (21)
$=\frac{1}{2}\,d_t^{Q}\,/\,q_{22}$	10^{-5}	-3.139 4 (30)	$=\frac{1}{2}\,d_t^{L}\,/\,q_{22}$	10^{-5}	4.861 (21)
$q_{12}^{l,D}$	10^{-6} cm^{-1}	3.052 (13)	q_{12}^{L}	10^{-6} cm^{-1}	-6.164 (16)
$=q_{12}^{l,Q}+\frac{Gd_t^{Q}}{4q_{22}}$	10^{-6} cm^{-1}	3.069 (13)	$=q_{12}^{D}+\frac{F}{G}q_{12}^{l,D}$	10^{-6} cm^{-1}	-6.180 (16)
$-8(\,q_{12}^{D})^2\,/\,F$	10^{-10} cm^{-1}	3.050 4 (59)	$-8(\,q_{12}^{L})^2\,/\,F$	10^{-9} cm^{-1}	1.981 (11)
$=-\frac{1}{2}F(\,d_t^{Q})^2\,/\,q_{22}^2$	10^{-10} cm^{-1}	3.024 1 (58)	$=-8F(\,q_{12}^{l,Q})^2\,/\,G^2$	10^{-9} cm^{-1}	1.998 (11)
$=(\eta_J^{Q}-\eta_J^{D})$	10^{-10} cm^{-1}	3.02 (84)	$=(\eta_J^{Q}-\eta_J^{L})$	10^{-9} cm^{-1}	1.980 (85)
$=-(\eta_K^{Q}-\eta_K^{D})$	10^{-10} cm^{-1}	2.99 (106)	$=-(\eta_K^{Q}-\eta_K^{L})$	10^{-9} cm^{-1}	1.966 (107)

[a] $F = C-B + 2C\zeta$; $G = C\zeta + 2g_{II}$.

Table 5. Parameters of the (2,2), (3,0) and (4,-2) interactions (in MHz units) in the vibrational states v_6=1, v_3=v_6=1, and v_6=2 of $CH^{35}Cl_3$ (reduction *Q*)

Parameter	v_6=1[a]	v_3=v_6=1	v_6=2
q_{22}	-1.827 752 (19)	-1.813 154 (18)	-1.829 780 3 (76)
$f_{22}^J \times 10^6$	3.855 2 (43)	4.052 9 (21)	3.863 3 (14)
$d_t \times 10^4$	1.127 14 (15)	1.290 3 (27)	1.148 89 (111)
$f_{42} \times 10^7$	4.873 6 (60)	4.935 (59)	5.095 1 (44)

[a] Parameters taken from [12].

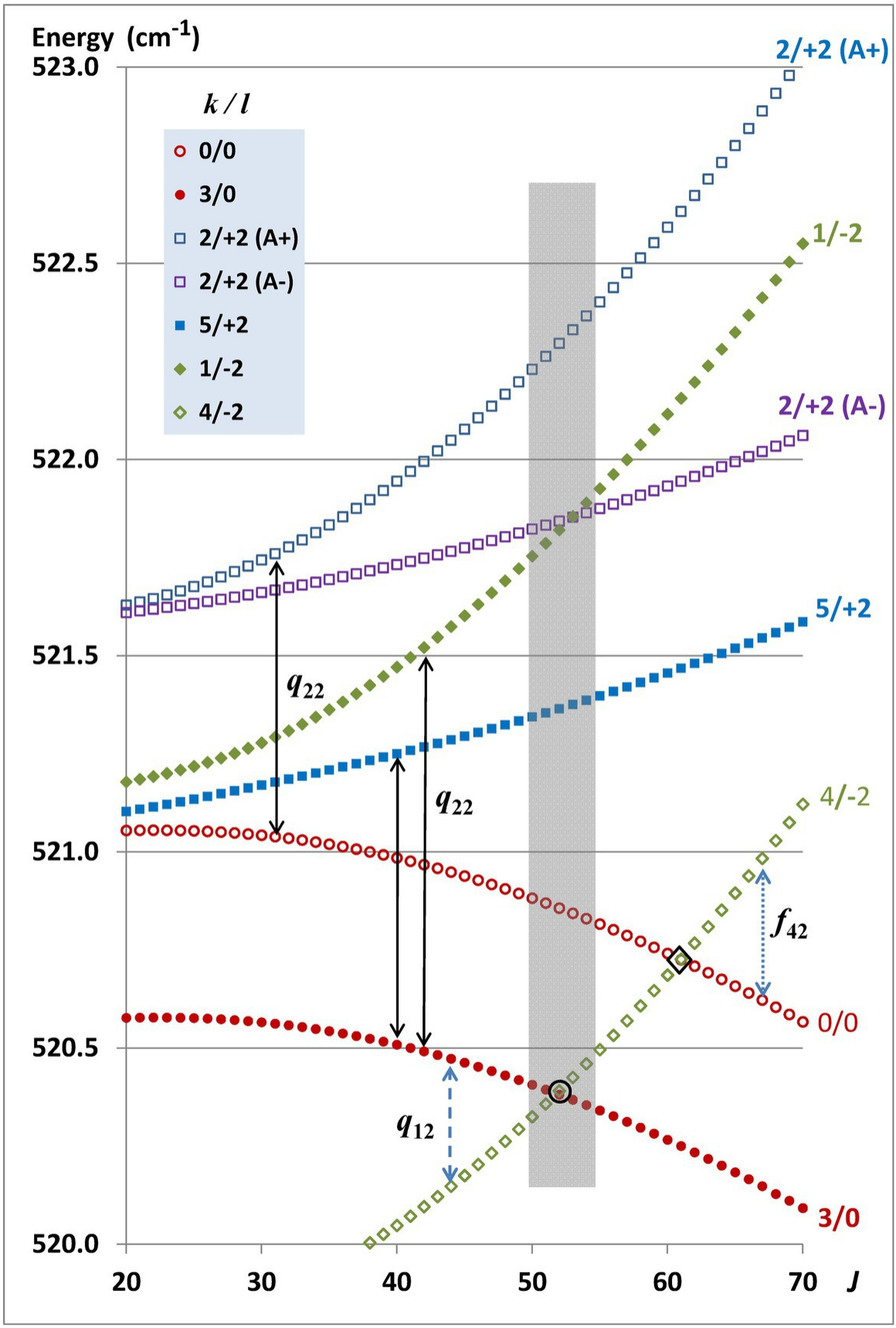
Energy (cm-1)
523.0
522.5
522.0
521.5
521.0
520.5
520.0
20
30
40
50
60
70
J
k / l
0/0
3/0
2/+2 (A+)
2/+2 (A-)
5/+2
1/-2
4/-2
2/+2 (A+)
1/-2
2/+2 (A-)
5/+2
4/-2
0/0
3/0
q22
q22
q12
f42